TITLE PAGE

Visual speed compensation of pitch-constrained blue-bottle flies under retinal-image velocity perturbation in a flight mill

Shih-Jung Hsu[1] and Bo Cheng[*,1]

[1]Department of Mechanical Engineering, Pennsylvania State University, University Park, PA 16802, USA

*Author for correspondence (buc10@psu.edu)

Keywords: visual control, optic flow, insect flight, locomotor constraint

Running title: Visual speed compensation of flies

ABSTRACT

In the presence of wind or background image motion, flies are able to maintain a constant retinal-image velocity via regulating flight speed to the extent permitted by their locomotor capacity. Here we investigated the speed regulation of semi-tethered blue-bottle flies (*Calliphora vomitoria*) flying along an annular corridor in a magnetically levitated flight mill enclosed by two motorized cylindrical walls. We perturbed the flies' retinal-image motion via spinning the cylindrical walls, generating bilaterally-averaged velocity perturbations from -0.3 to 0.3 $m \cdot s^{-1}$. Flies compensated retinal-image velocity perturbations by adjusting airspeed up to 20%, thereby maintaining a relatively constant retinal-image velocity. When the retinal-image velocity perturbation became greater than ~0.1 $m \cdot s^{-1}$, the compensation weakened as airspeed plateaued, suggesting that flies were unable to further change airspeed. The compensation gain, i.e., the ratio of airspeed compensation and retinal-image velocity perturbation, depended on the spatial frequency of the grating patterns, being the largest at 12 m^{-1}.

INTRODUCTION

Flying insects rely heavily on retinal-image motion to control their flight (Borst et al., 2010; Srinivasan and Zhang, 2004). They often regulate flight speed by maintaining a constant retinal-image velocity (or optic flow) (David, 1982; Serres et al., 2008; Srinivasan et al., 1996; Srinivasan et al., 2000), which can be extracted over a broad range of image spatiotemporal frequencies (Fry et al., 2009). This differs from the classical optomotor turning response to rotating grating patterns (Borst et al., 2010), which is sensitive to image temporal frequency that depends on the image spatial frequency at a given retinal-image velocity.

Visual control of forward flight in insects is commonly studied using flight tunnels in free-flight (David, 1982; Fuller et al., 2014; Serres et al., 2008; Srinivasan et al., 1996) or tethered-flight settings (David, 1978; Lawson and Srinivasan, 2017). Recent efforts by the authors also demonstrated the potential of using flight mills to study forward flight in semi-tethered settings with controlled flight conditions (Hsu et al., 2019). While evidence has shown that free-flying insects in flight tunnels are able to maintain a constant retinal-image velocity in the presence of wind or background image motion (David, 1982; Srinivasan et al., 1996), it is unknown whether the same speed-regulation behavior also remains in semi-tethered flies in a flight mill.

Flying insects change their flight speed mainly through body-pitch dominated vectoring and magnitude modulation of cycle-averaged wing aerodynamic force, with a relatively small change in its direction relative to the body, a mechanism commonly described as the “helicopter model” (David, 1978; Muijres et al., 2014). However, it has been observed that insects can also change their flight speeds in the absence of any pitch maneuvers. For example, fruit flies can use a swimming-like paddling wing motion for thrust and speed modulation (Ristroph et al., 2011); and drone flies can produce significant airspeed changes, with negligible body pitch variations around

56 0°, at least for a short period of time (3-10 seconds) (Meng and Sun, 2016). As these relatively
57 scarce observations suggest that insects are at least capable of relying only on the changes in wing
58 motion to fly at different speeds, therefore do not have to conform to the helicopter model, it is
59 unclear if they still modulate flight speed to maintain a constant retinal-image velocity with a
60 constrained pitch, and to what extent can the changes of wing motion modulate speed before the
61 locomotor limit is reached.

62 In this study, we used a motorized magnetically levitated (MAGLEV) flight mill, modified
63 from those used in Hsu et al. (Hsu et al., 2019), to study the steady-state speed regulation in blue
64 bottle flies (*Calliphora vomitoria*). We aimed to address two questions: 1) whether flies attempt
65 to maintain a constant retinal-image velocity under retinal-image velocity perturbations when
66 flying in the flight mill? similar to those observed in free flight, and 2) whether and to what extent
67 can flies regulate flight speed using only the wing kinematic changes without body pitch change?
68 In the experiments, the flies were constrained at a fixed body pitch (0°) in an annular corridor
69 between two cylindrical walls displaying grating patterns, which generated retinal-image velocity
70 perturbations via their co-rotations at the same angular velocity. We quantified the flies' responses
71 in terms of the changes in airspeeds and retinal-image velocities, as functions of retinal-image
72 velocity perturbations.

73 **MATERIALS AND METHODS**

74 **(a) Motorized magnetic levitated (MAGLEV) flight mill apparatus**

75 A motorized MAGLEV flight mill (Fig. 1A), modified from that developed in Hsu and his
76 coworkers (Hsu et al., 2019), was used in this study. The flight mill shaft, with three permanent
77 magnets placed at its center, was levitated by two vertically aligned electromagnets. A
78 proportional-integral-derivative (PID) controller generated pulse width modulation (PWM) signals

to the electromagnets using the feedback of the permanent magnets' vertical position measured by a linear Hall effect sensor. The flies, tethered to one end of the shaft, flew in an annular corridor of the flight mill enclosed by an inner (diameter 0.254 m) and an outer (diameter 0.349 m) cylindrical wall, which were centered via a vertical metal post and were driven by stepper motors via timing gears and pulleys. Both cylindrical walls displayed vertical grating patterns with one of the three spatial frequencies (SF): 24, 12 and ~0 (no pattern) m^{-1}, i.e., the number of the grating cycles per meter. Note that all angular units in the paper were converted to linear units using the radius of the fly's circular path at the center of the annular corridor, which was 0.146 m. The syn-directional and anti-directional rotations of the cylindrical walls (or the translations of the grating patterns) relative to the flight direction of the flies, created perturbations to the fly's retinal-image velocity. We mounted two laser-and-photodiode pairs on the metal post with a 120° spacing (Fig. 1A), and we measured the average ground speed of the flies (V_g, the forward velocity of the fly with respect to the fixed laboratory frame) based on the time lapses of the shaft passing two of the laser-and-photodiode pairs. A light source was mounted on the top of the entire device to provide consistent lighting (2877 ± 868 lux) to the annular corridor.

(b) Animal preparation and experimental procedure

We used 4- to 8- days blue-bottle flies (*Calliphora vomitoria*) (N = 42, 32.9 ± 8.7 mg) for the experiments. Each fly was first cold anesthetized, while having its thorax glued orthogonally to a metal pin. The metal pin was then attached orthogonally to the flight mill shaft, therefore holding the fly at approximately 0° body pitch angle (Fig. 1A). After being introduced into the flight mill, the flies flew continuously in a clockwise direction at the middle of the annular corridor between the two cylindrical walls (Fig. 1A, also see Movie S1). Note that since the distance between the flies and the inner and outer walls were fixed for all experiments, the linear velocity of the grating

patterns on the rotating cylindrical walls was equivalent to the image velocity or the optical flow introduced to a fly's retina in our study. The retinal-image velocity perturbations were applied to each fly with a 0.03 $m \cdot s^{-1}$ interval following two sequences with opposite directions: 1) 0 → 0.3 → -0.3 → 0 $m \cdot s^{-1}$, and 2) 0 → -0.3 → 0.3 → 0 $m \cdot s^{-1}$. The results of one-way analysis of variance (ANOVA) test showed that for each SF group, the direction of the sequences has no significant effect on flies' mean forward velocity (Table S2). After each change of perturbation velocity, a fly's forward velocity was measured after 40 seconds of waiting period to ensure that the fly flew at near steady state. Note that in the experiment, individual flies were not distinguished.

As the two cylindrical walls spun, they induced air flow between them (i.e., Taylor–Couette flow (Taylor, 1923)). This wall-induced wind speed (V_w) led to a difference between the ground speed (directly measured) and the airspeed of the flies, and therefore needs to be considered in the calculation of the latter analysis. Therefore, V_w was measured for each perturbation velocity without the presence of the fly by a hot-wire anemometer (405i, testo, Lenzkirch, Germany) and was found linearly dependent on the spinning speed (Fig. S1).

(c) Data analyses and model selection

The responses of the flies to retinal-image velocity perturbations (V_c) were measured by the changes in their bilaterally-averaged retinal-image velocity (ΔV_r) and the changes in their airspeed (ΔV_a). The bilaterally-averaged retinal-image velocity (V_r) perceived by the fly, which was equivalent to the relative groundspeed between the fly and the cylindrical walls, was calculated by,

$$V_r = V_g - V_c, \tag{1}$$

where V_g was the measured groundspeed and V_c was the bilaterally-averaged linear velocity of the grating patterns on inner and outer walls, which was equal to the product of the angular velocity of the cylindrical walls and the radius of the fly's circular path at the center of the annular corridor.

Note that in this study, we didn't distinguish the retinal-image velocities between the two eyes of the flies, as both V_r and V_c were considered bilaterally averaged.

The fly's airspeed (V_a) was calculated based on the groundspeed (V_g) and the wall-induced wind speed (V_w),

$$V_a = V_g - V_w. \tag{2}$$

Note that we used the airspeed instead of the groundspeed in our analysis because the former better reflected the biomechanical efforts or the constraints of the flies in the compensation of the perturbation.

Assuming the existence of visual speed compensation, a fly would change its airspeed (or groundspeed) in the same direction of the retinal-image velocity perturbation, thereby keeping its retinal-image velocity near constant (or $\Delta V_r \approx 0$) (Fig. 1C). In addition, assuming that the changes of the airspeed (ΔV_a) would saturate due to biomechanical constraints when the magnitude of the perturbation (V_c) became sufficiently large, the flies would not be able to indefinitely increase or decrease their airspeed once it reached to an upper or lower bound, respectively. As a result, the ΔV_r would eventually increase (or decrease) with V_c as no further compensation would be possible.

Therefore, to model the flies' response ΔV_r as a function of V_c, we performed nonlinear regressions and model selection on two competing explanatory models developed assuming the existence or nonexistence of visual speed compensation, i.e., a linear function model ($M_{\Delta V_r}^{linear}$) (assuming no visual compensation) and a cubic function model ($M_{\Delta V_r}^{cubic}$) (assuming the existence of visual compensation). The cubic function was defined as,

$$\Delta V_r(V_c) = V_r - V_{r0} = \beta_0 + \beta_3(V_c - c)^3, \tag{3}$$

143 where V_{r0} was the measured mean retinal-image velocity of the flies without perturbation for each
144 trial, β_0 and β_3 are the coefficients of polynomials, and c is the inflection point, β_0, β_3, and c were
145 obtained from nonlinear regression.

146 To model the flies' response ΔV_a as a function of V_c, we also performed nonlinear regressions
147 and model selection on two explanatory models: a linear function model ($M_{\Delta V_a}^{linear}$, assuming no
148 airspeed saturation) and a generalized logistic function model (Richards, 1959) ($M_{\Delta V_a}^{logistic}$)
149 (assuming airspeed saturation). The generalized logistic function is defined as:

$$\Delta V_a(V_c) = V_a - V_{a0} = \Delta V_a^{min} + \frac{\Delta V_a^{max} - \Delta V_a^{min}}{1+e^{-\beta(V_c-c)\gamma}}, \quad (4)$$

150 where V_{a0} was the measured mean airspeed of the flies without perturbation of each trial, ΔV_a^{min}
151 and ΔV_a^{max} were the lower and upper asymptotic bounds, representing the minimal and maximum
152 change in airspeed, respectively, β is the growth rate, c is where the maximum growth rate occurs
153 and γ is the asymmetry coefficient (Richards, 1959). We also defined the compensation gain as
154 the ratio between changes of airspeed and image-velocity perturbation, evaluated locally at $V_c = 0$:

155 $$K_c = \left.\frac{\mathrm{d}(\Delta V_a)}{\mathrm{d}V_c}\right|_{V_c=0}, \quad (5)$$

156 which was simply the slope for $M_{\Delta V_a}^{linear}$ and the first derivative of $M_{\Delta V_a}^{logistic}$ at $V_c = 0$.

157 We used the Levenberg-Marquardt algorithm (Elzhov et al., 2015) for the nonlinear regression
158 to find the best fit for each model. Finally, the models were compared using Akaike information
159 criterion (AIC) (Akaike, 1998), which evaluated the trade-off between the goodness-of-fit and the
160 simplicity of the model.

161 RESULTS AND DISCUSSION

162 42 blue-bottle flies (32.9 ± 8.7 mg) were used in the experiments, producing 2,228 measurements
163 of flight speeds for the 21 cases of retinal-image perturbation (V_c) ranging from -0.3 m·s^{-1} to 0.3

m·s^{-1} (see the sample size for each case in Table S1). The groundspeed (V_g) at V_c = 0 was 0.44 ± 0.12 m·s^{-1} (Fig. S2) (no significant effect of SF on V_g at the p<.05 level [$F_{2, 201}$ = 1.304, p = 0.274]).

When V_c were relatively small (-0.12 < V_c < 0.10 m·s^{-1}, Fig. 2B), the flies well compensated the perturbations at SF = 12 m^{-1} by keeping retinal-image velocity approximately constant ($\Delta V_r \approx 0$) (Fig. 2A). The compensations existed but were significantly weaker at the higher (SF = 24 m^{-1}) or lower (SF ~ 0 m^{-1}) SF (Fig. 2A), both of which resulted in a near linear trend of ΔV_r in response to V_c. When the magnitude of the perturbations became large, the compensation in SF = 12 m^{-1} group also begun to weaken as ΔV_r started to change linearly in the opposite direction of perturbation V_c.

The observed compensation to maintain $\Delta V_r \approx 0$ was mainly the result of the changes in flies' airspeed in response to the perturbation, as flies changed their airspeed in the same direction of the perturbation. This was confirmed by the monotonically trends of ΔV_a with V_c for all three SF cases (Fig. 2B). The compensation gain was significantly higher for SF = 12 m^{-1} (K_c = 0.868), compared with those of SF = 0 m^{-1} (K_c = 0.233) and SF = 24 m^{-1} (K_c = 0.337). The airspeed changes exhibited saturation under large perturbations, most apparently for SF = 12 and 24 m^{-1} (Fig. 2B). For SF = 24 m^{-1}, the upper and lower bounds of ΔV_a were 0.034 ± 0.009 m·s^{-1} (mean ± 95% confidence interval (CI)) and -0.089 ± 0.010 m·s^{-1} (mean ± 95% CI), respectively. For SF=12 m^{-1}, the upper and lower bounds of ΔV_a were 0.095 ± 0.010 m·s^{-1} and -0.091 ± 0.014 m·s^{-1} (mean ± 95% CI).

Consistent with the above observations, the model selection results (Table 1) showed that for SF = 12 m^{-1} the AIC favored models that assumed the existence of visual speed compensation and airspeed saturation, i.e., $M_{\Delta V_r}^{cubic}$ and $M_{\Delta V_a}^{logistic}$, while for SF = 0 m^{-1} the AIC favored the models assuming no compensation and no airspeed saturation, i.e., $M_{\Delta V_a}^{linear}$, $M_{\Delta V_r}^{linear}$. For SF = 24 m^{-1}, AIC

186 favored the model that assumed no visual speed compensation $M_{\Delta V_r}^{linear}$ and the model that assumed
187 the existence of airspeed saturation $M_{\Delta V_a}^{logistic}$.

188 In this work, we studied the responses of blue-bottle flies (*Calliphora vomitoria*) subjected to
189 retinal-image velocity perturbation while flying in the motorized MAGLEV flight mill with a
190 constrained pitch. Similar to those observed in free-flight conditions (David, 1982; Serres et al.,
191 2008; Srinivasan et al., 1996; Srinivasan et al., 2000), the flies appeared to compensate retinal-
192 image velocity perturbations by changing their airspeed (or groundspeed) syn-directionally with
193 the perturbation. The compensation was the strongest for perturbations between -0.12 $m \cdot s^{-1}$ and
194 0.10 $m \cdot s^{-1}$ at SF = 12 m^{-1}, corresponding to a compensation gain at 0.868, significantly higher than
195 those for SF = ~0 and 24 m^{-1}. The observed dependency on image spatial frequency in the speed
196 compensation responses was similar to those identified in the free-flight acceleration responses of
197 fruit flies (*Drosophila melanogaster*) (Fry et al., 2009), which showed that the response strength
198 was among the strongest at SF of 12 m^{-1}, but reduced substantially at 24 m^{-1}. Nevertheless,
199 compared with classical optomotor turning response (Borst et al., 2010), it is expected that the
200 dependency on spatial frequency in speed compensation or acceleration responses is relatively
201 weak, because the retinal-image velocity can be extracted robustly over a broad range of image
202 spatiotemporal frequencies (Fry et al., 2009), while the optomotor turning response is proportional
203 to image temporal frequency that depends on image spatial frequency at a fixed image velocity
204 (Borst et al., 2010).

205 When the magnitude of the retinal-image velocity perturbation became large, speed
206 compensation weakened as the changes in airspeed plateaued, as flies were unable to adjust their
207 airspeed beyond approximately ±0.1 $m \cdot s^{-1}$ (or +22% and -21% compared to the average airspeed
208 at V_c = 0 under SF = 12 m^{-1}). This was possibly due to a compound of biomechanical constraints,

including the constrained pitch and their force-vectoring ability via changes of wing motion (Hsu et al., 2019). Note that the current studies were limited to the steady-state responses, while flies are likely capable of large transient modulation of wing motion during rapid aerodynamic maneuvers and flight stabilization (Ristroph et al., 2010). It can be also speculated that with a free body pitch, e.g., by tethering a fly to the flight mill via a micro bearing, the successful compensation region (Fig. 2B) can be further expanded to larger image-velocity perturbations.

In conclusion, to address the two motivating questions of this study, our results showed that 1) when flying in the MAGLEV flight mill, flies did regulate their flight speed to maintain a constant retinal-image velocity under image velocity perturbations, similar to those observed in free flight, and 2) flies were capable of adjusting flight speed using only the wing kinematic changes during steady-state flight, however the amount of adjustment was relatively small (less than 0.1 m/s).

ACKNOWLEDGEMENTS

We thank Elizabeth Seber and Ciera McFarland for the assistance with the experiments.

COMPETING INTERESTS

The authors declare no competing or financial interests.

AUTHOR CONTRIBUTIONS

S.J.H. and B.C. contributed to the design of the experiments, data analysis, interpretation of the findings and the manuscript preparation. S.J.H. prepared and conducted the experiments.

FUNDING

This research was supported by the National Science Foundation (CMMI 1554429 to B.C.).

SUPPLEMENTARY INFORMATION

Supplementary information available online at
http://jeb.glologists.org/lookup/doi/xxx/xxx.supplemental

REFERENCES

Akaike, H. (1998). Information Theory and an Extension of the Maximum Likelihood Principle. In *Selected Papers of Hirotugu Akaike*, pp. 199–213. Springer, New York, NY.

Borst, A., Haag, J. and Reiff, D. F. (2010). Fly motion vision. *Annu. Rev. Neurosci.* **33**, 49–70.

David, C. T. (1978). The relationship between body angle and flight speed in free flying Drosophila. *Physiol. Entomol.* **3**, 191–195.

David, C. T. (1982). Compensation for height in the control of ground speed by Drosophila in a New, "Barber's Pole" wind tunnel. *J. Comp. Physiol. A* **147**, 485–493.

Elzhov, T. V., Mullen, K. M., Spiess, A.-N. and Bolker, B. (2015). minpack. lm: R interface to the Levenberg-Marquardt nonlinear least-squares algorithm found in MINPACK, plus support for bounds (Ver. 1.2-0) R package.

Fry, S. N., Rohrseitz, N., Straw, A. D. and Dickinson, M. H. (2009). Visual control of flight speed in Drosophila melanogaster. *J. Exp. Biol.* **212**, 1120–1130.

Fuller, S. B., Straw, A. D., Peek, M. Y., Murray, R. M. and Dickinson, M. H. (2014). Flying Drosophila stabilize their vision-based velocity controller by sensing wind with their antennae. *Proc. Natl. Acad. Sci.* **111**, E1182—-E1191.

Hsu, S.-J., Thakur, N. and Cheng, B. (2019). Speed control and force-vectoring of bluebottle flies in a magnetically levitated flight mill. *J. Exp. Biol.* **222**, jeb187211.

Lawson, K. K. K. and Srinivasan, M. V. (2017). Flight control of fruit flies: dynamic response to optic flow and headwind. *J. Exp. Biol.* **220**, 2005–2016.

Meng, X. G. and Sun, M. (2016). Wing and body kinematics of forward flight in drone-flies. *Bioinspir. Biomim.* **11**, 056002.

Muijres, F. T., Elzinga, M. J., Melis, J. M. and Dickinson, M. H. (2014). Flies evade looming targets by executing rapid visually directed banked turns. *Science* **344**, 172–177.

Richards, F. (1959). A flexible growth function for empirical use. *J. Exp. Bot.* **10**, 290–301.

Ristroph, L., Bergou, A. J., Ristroph, G., Coumes, K., Berman, G. J., Guckenheimer, J., Wang, Z. J. and Cohen, I. (2010). Discovering the flight autostabilizer of fruit flies by inducing aerial stumbles. *Proc. Natl. Acad. Sci.* **107**, 4820–4824.

Ristroph, L., Bergou, A. J., Guckenheimer, J., Wang, Z. J. and Cohen, I. (2011). Paddling mode of forward flight in insects. *Phys. Rev. Lett.* **106**, 1–4.

Serres, J. R., Masson, G. P., Ruffier, F. and Franceschini, N. (2008). A bee in the corridor: centering and wall-following. *Naturwissenschaften* **95**, 1181–1187.

Srinivasan, M. V. and Zhang, S. (2004). Visual motor computations in insects. *Annu. Rev. Neurosci.* **27**, 679–696.

Srinivasan, M. V., Zhang, S., Lehrer, M. and Collett, T. S. (1996). Honeybee navigation en route to the goal: visual flight control and odometry. *J. Exp. Biol.* **199**, 237–44.

Srinivasan, M. V., Zhang, S.-W., Chahl, J. S., Barth, E. and Venkatesh, S. (2000). How honeybees make grazing landings on flat surfaces. *Biol. Cybern.* **83**, 171–183.

Taylor, G. I. (1923). VIII. Stability of a viscous liquid contained between two rotating cylinders. *Philos. Trans. R. Soc. Lond. Ser. Contain. Pap. Math. Phys. Character* **223**, 289–343.

FIGURES

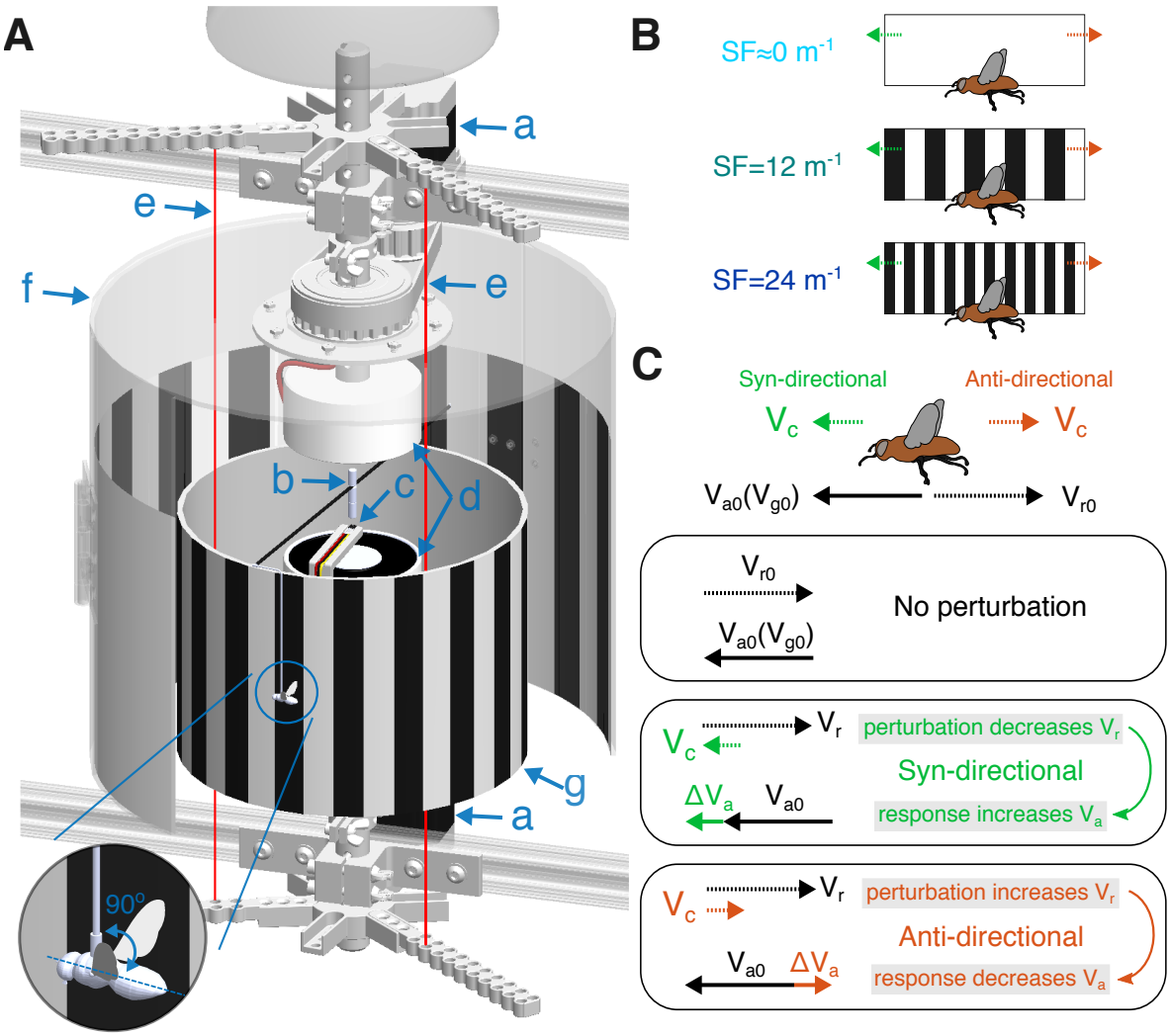

Figure 1. Experimental apparatus and methods. (A) The design of the MAGLEV flight mill system: a) timing gears, pulleys and stepper motors, b) permanent magnets and mill rotating shaft, c) Hall effect sensor, d) electromagnets, e) laser-and-photodiode pairs, f) outer and g) inner cylindrical walls with squared wave grating patterns. Magnified cutaway view: blue-bottle fly tethered at 0° body pitch with an angle pin. (B) Grating patterns with three spatial frequencies (SF=~0, 12 and 24 m^{-1}) used in the experiments. (C) Retinal-image velocity perturbations (V_c) are given syn-directionally (green dotted arrow) or anti-directionally (red dotted arrow). With no perturbation, the fly flies with an airspeed V_{a0} (same as ground speed V_{g0}) generating an opposite retinal-image velocity V_{r0}. Syn-directional (anti-directional) perturbation V_c decreases (increases) the retinal-image velocity V_r, which is compensated by the fly via increasing (decreasing) its airspeed (ΔV_a).

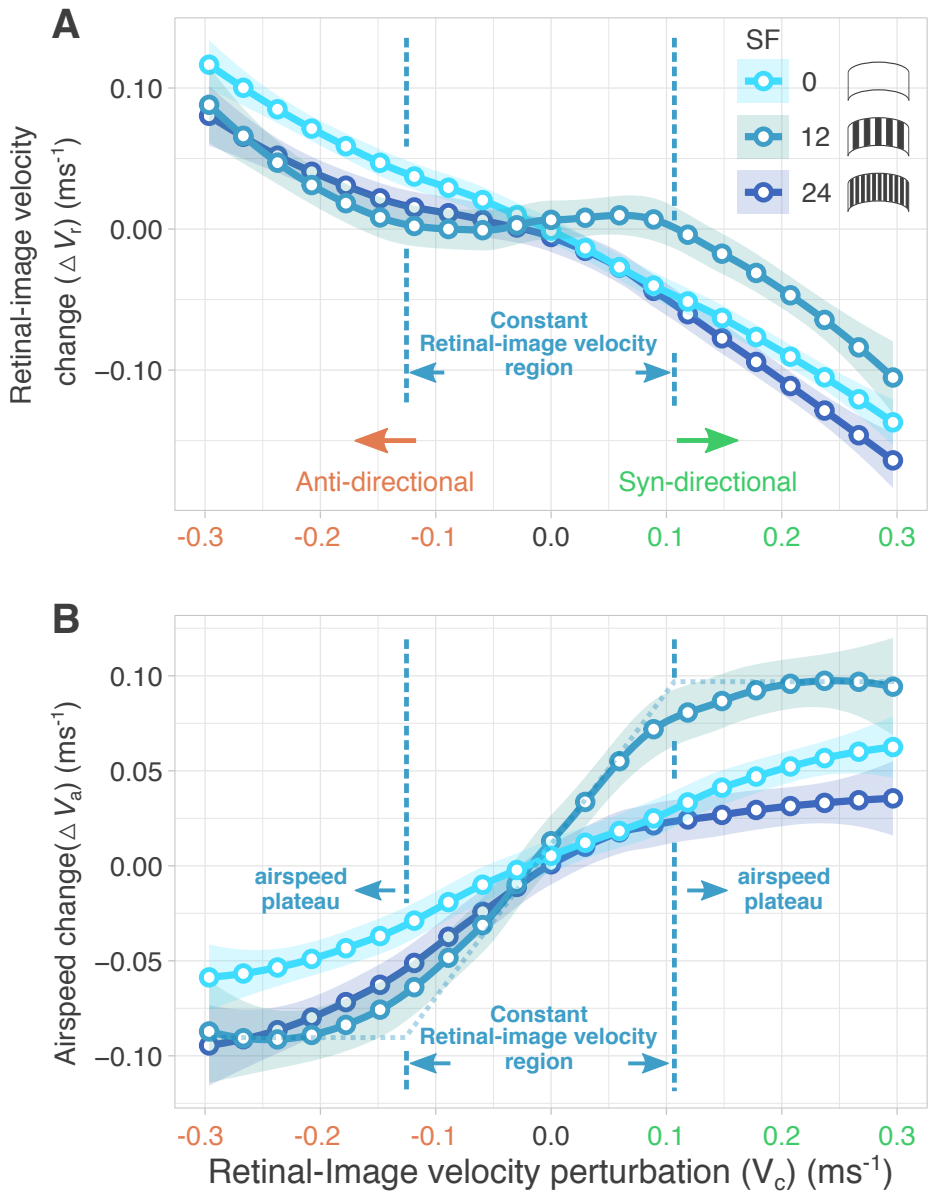

Figure 2. Flies' responses under retinal-image velocity perturbation. (A) The change of flies' retinal-image velocity (ΔV_r) in response to the perturbation (V_c). (B) The change of flies' airspeed (ΔV_a) in response to the perturbation (V_c). Solid lines and shades represent LOESS regression mean and 95% confidence interval, respectively. Airspeed plateaued (at SF = 12) when retinal-image velocity perturbation is above 0.10 m·s^{-1} or below -0.12 m·s^{-1} (calculated by intersecting of the asymptote lines and the tangent line at the inflection point based on the data of SF=12 m^{-1}. Teal dotted line in (B)). Between these two bounds (vertical dashed lines), blue bottle flies successfully maintained a constant retinal-image velocity. Horizontal green and red arrows indicate the syn-directional and the anti-directional image-velocity perturbations, respectively. Visual speed compensation corresponds to a syn-directional change of flies' airspeed or groundspeed with respect to the perturbation, regardless of the perturbation is syn-directional or anti-directional to the flies absolute airspeed or groundspeed.

TABLES

Table 1. Model selection results based on Akaike's information criterion (AIC). $M_{\Delta V_r}^{cubic}$ and $M_{\Delta V_r}^{linear}$ are the models for the retinal-image velocity response (ΔV_r) assuming the existence and the nonexistence of visual speed compensation, respectively. $M_{\Delta V_a}^{logistic}$ and $M_{\Delta V_a}^{linear}$ are models for the airspeed response (ΔV_a) assuming the existence and the nonexistence of airspeed saturation, respectively. The selected models are highlighted in light gray. Nonlinear regression results are shown in Table S3.

Retinal-image velocity change (ΔV_r)	Model		d.f.	Loglikely-hood	AIC	AIC weights
SF=24 m^{-1}	$M_{\Delta V_r}^{cubic}$	$\Delta V_r = \beta_0 + \beta_3(V_c - c)^3$	3	798.05	-1588.09	<0.01
	$M_{\Delta V_r}^{linear}$	$V_r = \beta V_c + c$	2	**807.39**	**-1608.79**	**>0.99**
SF=12 m^{-1}	$M_{\Delta V_r}^{cubic}$	$\Delta V_r = \beta_0 + \beta_3(V_c - c)^3$	3	**560.03**	**-1112.07**	**>0.99**
	$M_{\Delta V_r}^{linear}$	$V_r = \beta V_c + c$	2	550.12	-1094.23	<0.01
SF=0 m^{-1}	$M_{\Delta V_r}^{cubic}$	$\Delta V_r = \beta_0 + \beta_3(V_c - c)^3$	3	1008.99	-2009.98	<0.01
	$M_{\Delta V_r}^{linear}$	$V_r = \beta V_c + c$	2	**1048.20**	**-2090.40**	**>0.99**
Airspeed change (ΔV_a)	Model		d.f.	Loglikely-hood	AIC	AIC weights
SF=24 m^{-1}	$M_{\Delta V_a}^{logistic}$	$\Delta V_a = \Delta V_a^{min} + \frac{\Delta V_a^{max} - \Delta V_a^{min}}{1 + e^{-\beta(V_c - c)^\gamma}}$	5	**820.98**	**-1629.95**	**>0.99**
	$M_{\Delta V_a}^{linear}$	$V_a = \beta V_c + c$	2	534.07	-1615.04	<0.01
SF=12 m^{-1}	$M_{\Delta V_a}^{logistic}$	$\Delta V_a = \Delta V_a^{min} + \frac{\Delta V_a^{max} - \Delta V_a^{min}}{1 + e^{-\beta(V_c - c)^\gamma}}$	5	**562.41**	**-1112.82**	**>0.99**
	$M_{\Delta V_a}^{linear}$	$V_a = \beta V_c + c$	2	550.29	-1094.58	<0.01
SF=0 m^{-1}	$M_{\Delta V_a}^{logistic}$	$\Delta V_a = \Delta V_a^{min} + \frac{\Delta V_a^{max} - \Delta V_a^{min}}{1 + e^{-\beta(V_c - c)^\gamma}}$	5	1050.81	-2089.62	0.27
	$M_{\Delta V_a}^{linear}$	$V_a = \beta V_c + c$	2	**1048.82**	**-2091.63**	**0.73**

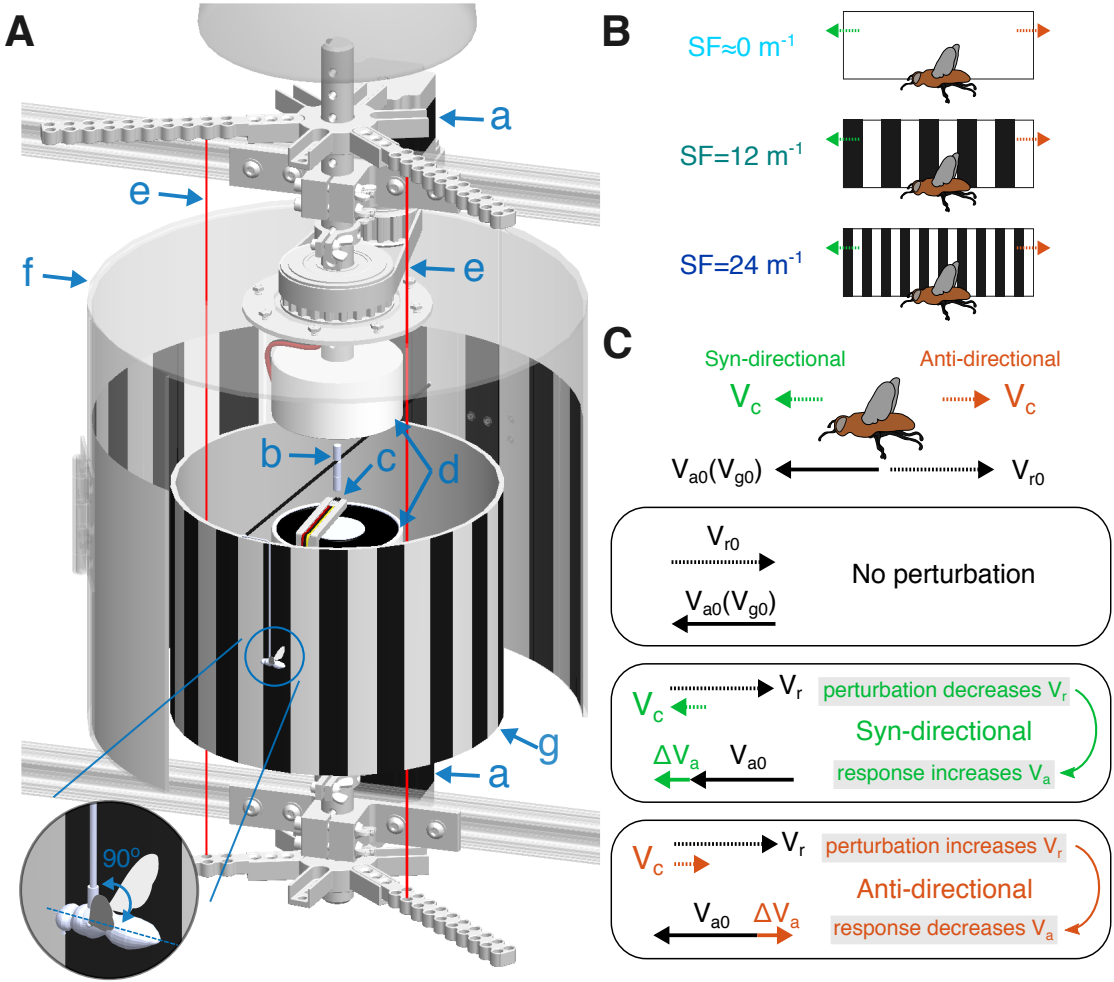
A
a
e
f
e
b
c
d
g
a
90°
B
SF≈0 m-1
SF=12 m-1
SF=24 m-1
C
Syn-directional
Anti-directional
Vc
Vc
Va0(Vg0)
Vr0
Vr0
Va0(Vg0)
No perturbation
Vc
Vr
perturbation decreases Vr
Syn-directional
ΔVa
Va0
response increases Va
Vc
Vr
perturbation increases Vr
Anti-directional
Va0
ΔVa
response decreases Va

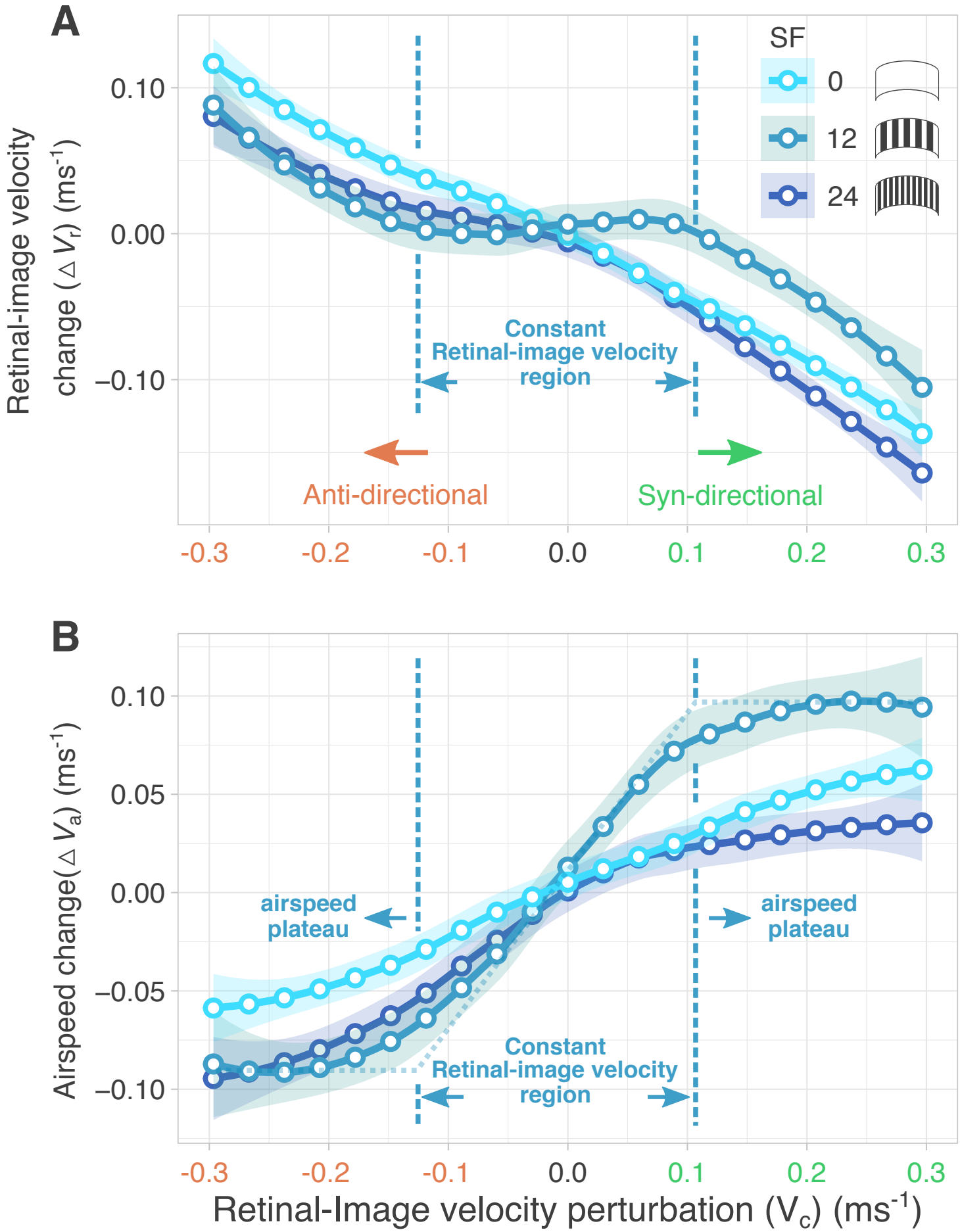
A
SF
0
12
24
Retinal-image velocity change (ΔV_r) (ms^{-1})
0.10
0.00
−0.10
Constant Retinal-image velocity region
Anti-directional
Syn-directional
-0.3
-0.2
-0.1
0.0
0.1
0.2
0.3
B
Airspeed change(ΔV_a) (ms^{-1})
0.10
0.05
0.00
−0.05
−0.10
airspeed plateau
airspeed plateau
Constant Retinal-image velocity region
-0.3
-0.2
-0.1
0.0
0.1
0.2
0.3
Retinal-Image velocity perturbation (V_c) (ms^{-1})